CFD and EnKF coupling estimation of LNG leakage and dispersion

Wu, Jiansong; Cai, Jitao; Yuan, Shuaiqi; Zhang, Xiaole; Reniers, Genserik

DOI
10.1016/j.ssci.2021.105263

Publication date
2021

Document Version
Accepted author manuscript

Published in
Safety Science

CFD and EnKF coupling estimation of LNG leakage and dispersion

Abstract: As a kind of clean fuel, increasing quantities of natural gas have been transported as liquefied natural gas (LNG) worldwide. The safety of LNG storage has gained the concerns from the public due to the potential severe consequences that may arise from LNG leakage. In this paper, a three-dimensional model with the combination of computational fluid dynamics (CFD) and the ensemble Kalman filter (EnKF) is proposed to predict LNG vapor dispersion and estimate the strength of the LNG leakage source. The LNG vapor dispersion CFD model is validated by the experimental data with good feasibility, and is further demonstrated with the reasonable modeling of the characteristics of the LNG vapor dispersion in a typical receiving terminal. The effectiveness of the proposed CFD and EnKF coupling model is evaluated and validated by a twin experiment. The results of the twin experiment indicate that the proposed CFD and EnKF coupling model allows the integration of observation data into the CFD simulations to enhance the prediction accuracy of the LNG vapor spatial-temporal distribution and thereby realizing a reasonable estimation of the LNG leakage velocity under complex environments. This study can provide technical supports for safety control, loss prevention and emergency response in case of LNG leakage accidents.

Keywords: LNG leakage; LNG vapor dispersion; LNG receiving terminal; computational fluid dynamics; ensemble Kalman filter

CFD and EnKF coupling estimation of LNG leakage and dispersion

Jiansong Wu[a], Jitao Cai[a], Shuaiqi Yuan[a,c,*], Xiaole Zhang[b], Genserik Reniers[c]

[a] School of Emergency Management & Safety Engineering, China University of Mining and Technology, Beijing 100083, China;

[b] Institute of Environmental Engineering, ETH Zürich, Zürich, CH-8093, Switzerland;

[c] Safety and Security Science Group, Faculty of Technology, Policy and Management, TU Delft, Delft, The Netherlands

*Corresponding author: cumtbyuanshuaiqi@163.com

CFD and EnKF coupling estimation of LNG leakage and dispersion

1. Introduction

The Liquefied Natural Gas (LNG) industry has attracted a lot of attention in the past few decades due to the increasing demand for clean energy all over the world. LNG receiving terminals that are equipped with large cryogenic storage tanks are regarded as an ideal way to satisfy the energy storage and energy supply (Lee et al., 2012; Li et al., 2012). As a kind of flammable and cryogenic gas, leaked LNG vapor could become a gas cloud rapidly because of the mass heat exchange with the atmospheric environment. There are possibilities of causing catastrophic consequences induced by the LNG tank leakage, such as cryogenic burns, fires, explosions, and so on. When serious LNG leakage accidents occur, the flammable gas cloud that formed by mixing natural gas and air could be driven by the ambient wind for several kilometers, which will pose serious threats to the human health and safety, and the environment. Meanwhile, the leaked LNG vapor will be driven by the negative buoyancy force because of the low temperature of LNG vapor at the initial stage of LNG leakage, which will aggravate the dangerous area (Pontiggia et al., 2009). As a result, the characteristics of LNG vapor dispersion, the prediction of the LNG vapor distribution and the estimation of the strength of the leakage source after LNG leakage have been a research focus in the past decade, which is of great significance for the loss prevention, safety control and emergency response of LNG leakage accidents.

In the early years, there were some studies investigating LNG spill accidents, which mainly focused on the field tests at relatively open terrains (Burro Series Data Report,1982; Coyote Series Data Report, 1983; Falcon Series Data Report, 1990). These experiments analyzed the process and characteristics of the LNG spilling on water and spreading with the ambient wind. Meanwhile, some Computational Fluid Dynamics (CFD) models have been developed for LNG spilling and dispersion simulation. Based on Coyote series experiments, Sklavounos et al. presented a comparison between ANSYS CFX and two popular box-models (SLAB and DEGADIS) by using statistical performance measures (Sklavounos et al., 2006). Cormier et al. (Cormier et al., 2009) and Qi et al. (Qi et al., 2010) employed the Brayton Fire Training Field (BFTF) experimental data to validate the ANSYS CFX code. Then, the process of LNG leakage and dispersion at a large pit with the consideration of the effects of dike wall/fence and the sensitivity analysis of several key parameters were investigated as well. The results indicated that the ANSYS CFX could obtain a good performance in the simulation of non-isothermal gas dispersion. What's more, the multi-phase of the LNG leakage process was taken into consideration in the previous studies. Giannissi et al. proposed a two-phase jet model, which could realize the simulation of LNG vapor dispersion and LNG liquid pool spreading simultaneously, and the Falcon series experiments were selected to validate the proposed two-phase model with good reliability (Giannissi et al., 2013). Additionally, the ANSYS FLUENT with the combination of the Lee model was proposed to simulate the LNG multi-phase

transformation process, which well predicted the peak value of LNG vapor compared with the Falcon series experimental data and other numerical models (Luo et al., 2018). However, the above studies mainly focused on the evaluation of the proposed CFD models by simplified experiments data without the consideration of the realistic complex layouts of a real LNG storage site. By contrast, Sun et al. (Sun et al., 2013) studied the LNG spill accident at an LNG station by using ANSYS FLUENT and assessed the risk of an LNG spill accident with the consideration of the influence of dyke walls. Similarly, Guo et al. utilized the Burro series test to evaluate the applicability of the Fluidyn-PANACHE code, and the effects of the atmosphere stability on the LNG vapor dispersion were discussed (Guo et al., 2019). Baalisampanga et al. (Baalisampanga et al., 2019) and Dasgotra et al. (Dasgotra et al., 2018) studied the LNG spilling accident using FLACS considering its cascading consequences, and the results showed that the integrated consequences were more severe.

However, there are always some uncertainties about the parameters of the LNG leakage source and dispersion process, which could bring a certain degree of errors to the simulation results. The LNG leakage rate and the ambient wind speeds under complex environments are difficult to estimate, which could result in a large deviation between simulation results and the real situations. Moreover, the estimation of LNG vapor leakage rate is of significance to provide technical supports for emergency response. The estimation of hazardous materials leakage source has been investigated by many studies. The data assimilation (DA) method is proven with good reliability

63 and practicability to estimate the strength of the leakage source and predict the
64 hazardous materials spatio-temporal distribution (Zhang et al., 2014; Xue et al., 2018;
65 Wu et al., 2018; Yuan et al., 2019). As a kind of sequential DA method, the ensemble
66 Kalman filter (EnKF) method is widely used in the prediction of hazardous materials
67 dispersion and with good feasibility to reconstruct hazardous materials release source
68 by integrating observation data into the dispersion models (Zhang et al., 2014; Yuan et
69 al., 2019). These studies demonstrate that the DA method and the ensemble Kalman
70 filter have great potentials in the prediction of LNG vapor dispersion and to realize the
71 estimation of the strength of the LNG vapor leakage source.

72 In this study, a three-dimensional CFD and EnKF coupling model is proposed to
73 estimate the LNG leakage and predict the LNG dispersion process. An OpenFOAM
74 solver is improved to simulate the LNG vapor dispersion process, and the EnKF method
75 is used to integrate the observation data into the OpenFOAM simulations and realize
76 the estimation of the leakage source at the same time. Firstly, the OpenFOAM solver
77 for simulating LNG vapor dispersion was evaluated and validated by using the Burro 8
78 spill test data. Furthermore, scenario analysis of LNG vapor leakage in an LNG
79 receiving terminal located in the north of China is conducted to investigate the
80 characteristics of LNG vapor dispersion in complex environments. Finally, a twin
81 experiment is done to evaluate and validate the proposed CFD and EnKF coupling
82 model through quantitative and qualitative analysis. This study could be helpful to
83 provide technical supports for safety control and emergency response of LNG leakage

accidents.

2. Methodology

2.1 Governing equations of LNG vapor dispersion

In this study, a three-dimensional compressible Navier-Stokes solver based on OpenFOAM is employed to simulate LNG vapor leakage and dispersion. This solver has been validated with feasibility and effectiveness in the simulation of gravity-driven gas flows (Fiates et al., 2016; Mack and Spruijt, 2013). In this paper, only the mass conservation equation, momentum conservation equation and no-reaction species mass-conservation equation are utilized, because there is no chemical reaction during the LNG vapor leakage and dispersion process. The basic governing equations of LNG vapor dispersion can be expressed as follows:

(i) Mass conservation equation

$$\frac{\partial \rho}{\partial \mathrm{t}} + \nabla \cdot (\rho \boldsymbol{v}) = 0 \quad (1)$$

(ii) Momentum conservation equation

$$\frac{\partial}{\partial \mathrm{t}}(\rho \boldsymbol{v}) + \nabla \cdot (\rho \boldsymbol{v}\boldsymbol{v}) = -\nabla p + \nabla \tau + \rho \boldsymbol{g} + \boldsymbol{F} \quad (2)$$

(iii) Species mass-conservation equation

$$\frac{\partial}{\partial \mathrm{t}}(\rho Y_i) + \nabla \cdot (\rho \boldsymbol{v} Y_i) = \nabla \cdot (D_C \nabla (\rho Y_i)) + S_i \quad (3)$$

where ρ is the density of the mixed gas, $\boldsymbol{v}$ is the velocity, p presents the pressure, and τ is the shear stress, which can be calculated according to the law of viscosity. $\boldsymbol{g}$ and

F present the gravity acceleration and the external forces respectively, and Y_i represents the volume concentration of different species. D_c represents the diffusion coefficient reflecting the gas diffusion degree and S_i represents the generalized source term.

2.2 Turbulence Model

The typical κ-ε turbulence model is widely applied in the CFD simulation of gas dispersion due to its stability and accurate prediction (Liu et al., 2018; Siddiqui et al., 2012). However, the standard κ-ε turbulence model has some shortages in handling fluid on the curved surface or even more complex flows. Therefore, the SST turbulence model was employed in this study that is a promising turbulence model in the simulation of gravity-driven gas flow with the combination of the advantages of the standard κ-ε model and the k–ω model (Li et al., 2016; Xing et al. 2013). The solved equations of the SST turbulence model are presented as follows:

$$\frac{\partial(\rho k)}{\partial t} + \nabla \cdot (\rho U k) = \nabla \cdot \left[\left(u + \frac{u_t}{\sigma_\omega}\right)\nabla k\right] + P_k - \beta' \rho k \omega \quad (4)$$

$$\frac{\partial(\rho \omega)}{\partial t} + \nabla \cdot (\rho U \omega) = \nabla \cdot \left[\left(u + \frac{u_t}{\sigma_\omega}\right)\nabla \omega\right] + \frac{\alpha\omega}{k} P_k - \beta \rho \omega^2 \quad (5)$$

$$\mu_t = \frac{\rho k}{\omega} \quad (6)$$

In the equations above, β', α, σ_k, σ_ω, and β are the model constants, which are assigned as $\beta' = 0.09, \alpha = \frac{5}{9}, \sigma_k = \sigma_\omega = 2, \beta = 0.075$ respectively according to a previous study (Sklavounos et al., 2006). κ means kinetic viscosity, ω represents the turbulent frequency, and P_k is the production rate of the turbulence. u_t represents turbulent

kinetic that can be calculated by using equation (6).

2.3 Ensemble Kalman Filter

The ensemble Kalman filter (EnKF) is a kind of widely-used data assimilation method, which can deal with the prediction of nonlinear dynamic models. It has some obvious advantages, such as consistent estimation of spatiotemporally varying model covariance, ease of implementation, and estimation of the posterior error (Pu and Hacker, 2009). The EnKF method has been widely used for solving many engineering problems, typically, it has already been successfully applied in the hydrological model prediction (Pu and Hacker, 2009; Valdes-Abellan et al., 2018), forecasting of smoke movement during tunnel fires (Ji et al., 2018), prediction of the indoor environment (Lin and Wang, 2013) and gas release and dispersion in an underground tunnel (Wu et al., 2018; Yuan et al., 2019). Meanwhile, the CFD and EnKF coupling model is also an alternative way to provide supports for the emergency of the nuclear accident (Zhang et al., 2015a; Zhang et al., 2015b).

In this study, the basic formulas of EnKF are described as follows:

$$y^f(t_i) = D\left(y^f(t_{i-1})\right) \tag{7}$$

$$y^a(t_i) = y^f(t_i) + E\left(r(t_i) - L\left(y^f(t_i)\right)\right) \tag{8}$$

Where y denotes the state vector, t_i and t_{i-1} represent the time step, $y^f(t_i)$ is the predicted value at time t_i, $y^a(t_i)$ is the analytical value at time t_i, D and L mean the nonlinear dynamic system model and the observation model respectively. r means the

observation vector and E denotes the ensemble Kalman gain.

EnKF describes the nonlinearity of the dynamic system by using a set of state estimations. The state matrix is generated as follows:

$$Y = \frac{1}{\sqrt{M-1}}(y_1, y_2, \ \ldots, \ y_M) \tag{9}$$

$$Y' = \frac{1}{\sqrt{M-1}}(y_1 - \bar{y}, \ y_2 - \bar{y}, \ \ldots, y_M - \bar{y}) \tag{10}$$

$$Q_e = Y'Y'^T \tag{11}$$

Where Y represents the state matrix, M is the ensemble size. Q_e denotes the ensemble covariance matrix, which is generated by the state ensemble. The ensemble Kalman gain and the prediction of the observation vector are calculated as follows:

$$r^f = L(y^f) \tag{12}$$

$$E = Q_e^f L^T (LQ_e^f L^T + Z_e)^{-1} \tag{13}$$

Where r^f means the prediction of the observation vector, and Z_e denotes the observation ensemble covariance matrix, which can be given as follows:

$$R = (r_o + \varepsilon_1 \ldots \ r_o + \varepsilon_n \ldots \ r_o + \varepsilon_M) \tag{14}$$

$$R' = (\varepsilon_1 \ \ldots \varepsilon_n \ \ldots \ \varepsilon_M) \tag{15}$$

$$Z_e = R'R'^T \tag{16}$$

Where ε_n is the pseudo-random perturbation. R indicates an ensemble of observation, which can be obtained by adding ε_n to the observation data r_o. Z_e represents the

161 covariance matrix of R'.

162 **2.4 State vector and update of source term**

163 In this paper, the state vector consists of the LNG vapor concentrations and the
164 leakage velocities:

165 $$y = (c_1 \dots c_i \dots c_n \;\; l_1 \dots l_j \dots l_m)^T \in R^{n+m} \tag{17}$$

166 Where *y* denotes the state vector, *c* means the concentration of the LNG vapor and *l*
167 means the LNG vapor leakage velocity at the leak hole. The subscript *n* and *m* represent
168 the number of LNG vapor concentrations and the number of data assimilation time steps
169 respectively.

170 $$l_j^b = \sum_{i=1}^{N} l_{j-1}^a(i) \,/M \tag{18}$$

171 $$l_j^f(i) = l_j^b + \delta l_j^b(i), \;\; i = 1,2,\dots,M \tag{19}$$

172 Where l_{j-1}^a means the latest updated leakage velocity ensemble, *i* and *M* represent the
173 ensemble member and ensemble size respectively. The ensemble l_1^f is the first-guess
174 leakage velocity, which can be initialed by the users. l_j^f represents a prior gas leakage
175 velocity for the j-th data assimilation, which are automatically calculated according to
176 the formulas (19). The added noise $\delta l_j^b(i)$ is generated as follows:

177 $$\delta l_j^b(i) = \alpha \delta l_{j-1}^a(i) + \sqrt{1-\alpha^2}\, c_j(i) \sigma_{j-1}^a, \;\; i = 1,2,\dots,M \tag{20}$$

178 Where $\delta l_{j-1}^a(i)$ denotes the deviation between the i-th analysis leakage velocity
179 and the ensemble mean σ_{j-1}^a represents the standard deviation, which is calculated by

l_{j-1}^{a}. $c_j(i)$ is random numbers, which following the Gaussian distribution *N (0,1)*. The parameter α (range from 0 to 1) controls the degree to which the influence of the prior state will be retained, which can be set as 0.99 in this paper.

2.5 CFD and EnKF coupling model for leakage source estimation and dispersion prediction

With the combination of LNG vapor dispersion model and EnKF algorithm, the CFD and EnKF coupling model for LNG vapor leakage source estimation and dispersion prediction are developed by the procedure shown in **Fig. 1**.

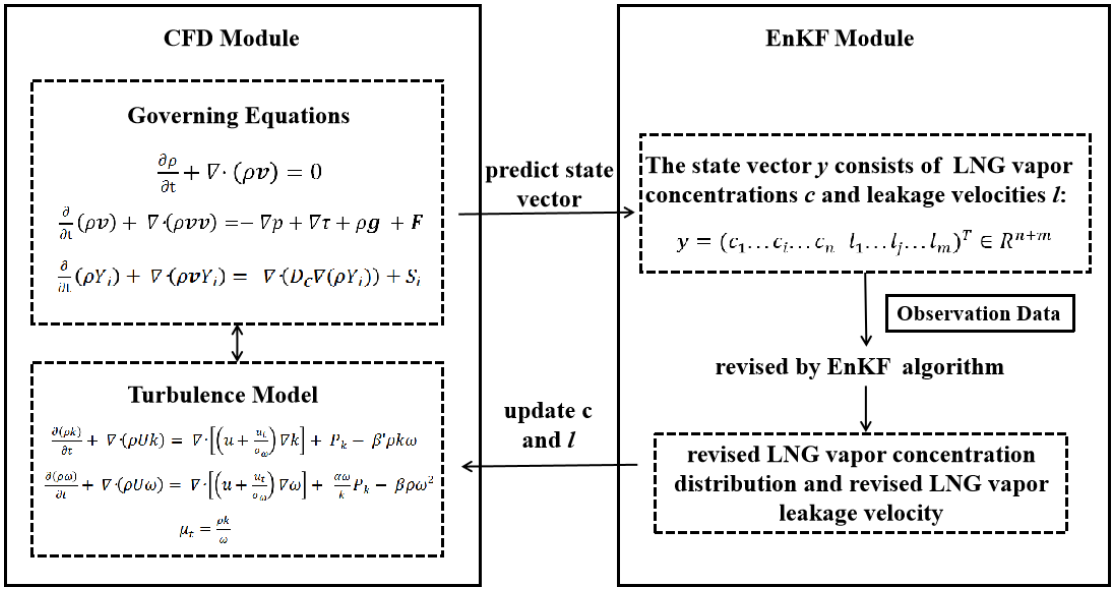

Fig. 1 Framework of the CFD and EnKF coupling model for LNG vapor leakage source estimation and dispersion prediction

The CFD and EnKF coupling model for leakage source estimation and dispersion prediction consists of the CFD module and the EnKF module. The CFD module is operated to simulate the LNG vapor dispersion process through the calculations of

governing equations and turbulence model. Meanwhile, the state vector of the EnKF module, which consists of LNG vapor concentrations and the leakage velocities in the leak hole can be predicted by the CFD module calculation. When the observation data is available, the state vector can be revised by the EnKF algorithm and the updates of the LNG vapor concentrations and the LNG vapor leakage velocities can be realized. Finally, the revised LNG vapor concentration distribution and the revised LNG vapor leakage velocity will be utilized into the CFD module for the next calculation of LNG vapor dispersion and a data assimilation step is finished.

3. Results and discussion

This section is organized as follows: Firstly, as a coupling model consisting of the CFD model and the EnKF algorithm, the feasibility of the CFD and EnKF coupling model can only be guaranteed after the validation of the CFD model. Therefore, the OpenFOAM-based CFD model was evaluated by experimental data firstly and then a case study was investigated as well to analyze the basic characteristics of the LNG vapor dispersion. Finally, the effectiveness of the proposed CFD and EnKF coupling model was demonstrated by a twin experiment.

3.1 Evaluation and validation of OpenFOAM code

As a kind of open-source CFD computing platform, OpenFOAM gained popularity in engineering system and scientific research. However, it has not been validated in a specific scenario associated with an LNG spill and vapor dispersion.

Moreover, the validation of the OpenFOAM code in the simulation of LNG vapor leakage and dispersion is of significance to the development of the CFD and EnKF coupling model LNG vapor leakage and dispersion prediction model, and it is also beneficial to provide an alternative tool for the investigation of LNG leakage and dispersion by numerical simulations. In this paper, the experimental data, the results of ANSYS FLUENT code and the results of the OpenFOAM code will be compared to validate the applicability of the OpenFOAM simulations.

3.1.1 Numerical configurations

The Burro 8 spill test performed by the Lawrence Livermore National Laboratory (LLNL) at the Naval Weapons Center was considered appropriate enough to investigate the behaviors and the characteristics of the LNG vapor dispersion due to its stable atmospheric conditions (Sun et al., 2013). In the Burro 8 test, the LNG vapor spread from a pond with a diameter of 58 m into the atmosphere environment. There were 25 gas sensor sites arranged downwind from the center of pond. 20 wind-filed station were placed in both upwind and downwind to capture the wind velocity and the wind directions. The experimental setup and the meteorological data involved in the Burro 8 experiment are listed in **Table.1**.

Table 1 Experimental setup and meteorological data involved in the Burro 8 experiment

Parameters	values
Spill volume (m^3)	28.4

Spill duration (s)	107
Spill rate (m^3/min)	16
Wind speed (m/s)	1.8
Ambient Temperature (°C)	33.1
Relative humidity	4.5 %
Atmospheric stability class	E
Monin-Obukhov length (m)	16.5

The computational domain used in the OpenFoam simulation was 1000_m×500_m×50_m. ANSYS ICEM was employed to create and discretize the computational domain. The hexahedral cells with refined mesh close to the pond and ground were used and the mesh in the computational domain can be seen in **Fig.2**.

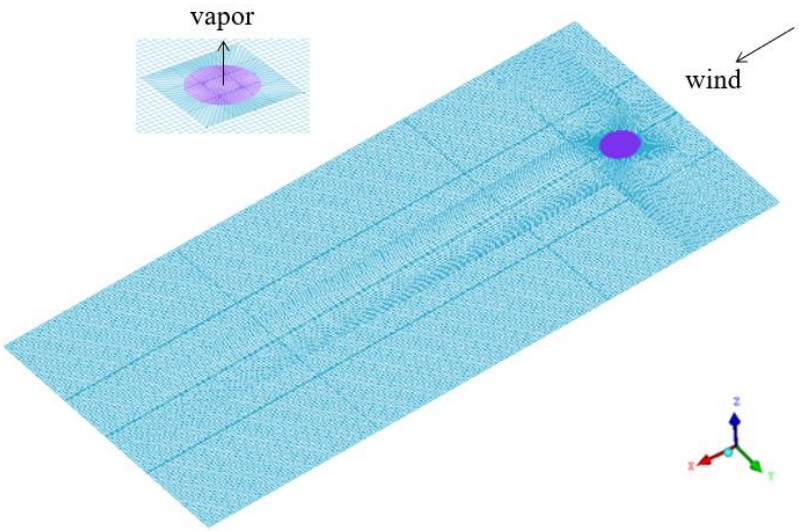

Fig.2 Mesh in the computational domain

According to the previous studies (Luo et al., 2018; Zhang et al., 2015), the boundary condition of velocity in the wind inlet was prescribed as uneven velocity inlet, which was calculated as follows:

$$U(z) = u_0 \times \left(\frac{z}{z_0}\right)^{\lambda} \quad (21)$$

where *U(z)* is the wind velocity at the specific height *z*, and u_0 is the reference velocity at the reference height z_0. In the Burro 8 test, u_0 was set as 1.8 m/s and z_0 was 2 m. λ is a dimensionless parameter determined by the atmospheric stability and the surface roughness, which was set as 0.12 in this study. This uneven velocity inlet was added into the OpenFOAM simulation by the codeFixedValue function in the OpenFOAM platform.

Due to the rapid evaporation phenomenon when LNG is spilt on a water pond area, the leakage velocity of the LNG vapor can be calculated by the formula as follows:

$$U_g = (\rho U)_{liq} / \rho_g, \quad (22)$$

Where U_g is the vapor leakage velocity in the computational domain, ρ_{liq} and ρ_g are the LNG density (424.1 kg/m^3) and the vapor density (1.76 kg/m^3) at 111 *K* respectively. U_{liq} represents LNG spill velocity, which can be calculated by the spill rate and the pond diameter.

The outflow boundary at 900 m downwind from the origin was set as pressure outlet, the top and the two sides of the computational domain were assumed far away from the vapor leakage area, which were set as symmetry boundary conditions. The ground was set as the wall with no-slip condition. Additionally, all the boundary conditions applied in the ANSYS FLUENT simulation were set according to the boundary conditions used in the OpenFOAM simulation.

3.1.2 Comparison and analysis

In order to obtain the mesh-independent simulation results, the mesh independence analysis was investigated by using four different meshes with grid numbers of 400 thousand, 550 thousand, 700 thousand and 850 thousand. Some sampling points obtained from a sampling line were selected to perform this mesh sensitivity analysis. The results of the calculated volume fraction of the LNG vapor at the sampling points by using four different meshes are shown in **Fig.3**. With the comparison between the results calculated by a different mesh, the average relative error and max error between mesh_1 and mesh_2 are 0.12 and 0.31 respectively. However, the average relative error and max error between mesh_2 and mesh_3 are 0.023 and 0.045 while 0.018 and 0.042 for mesh_3 and mesh_4. Therefore, mesh_2 was selected for the following simulation with both good accuracy and less computation load.

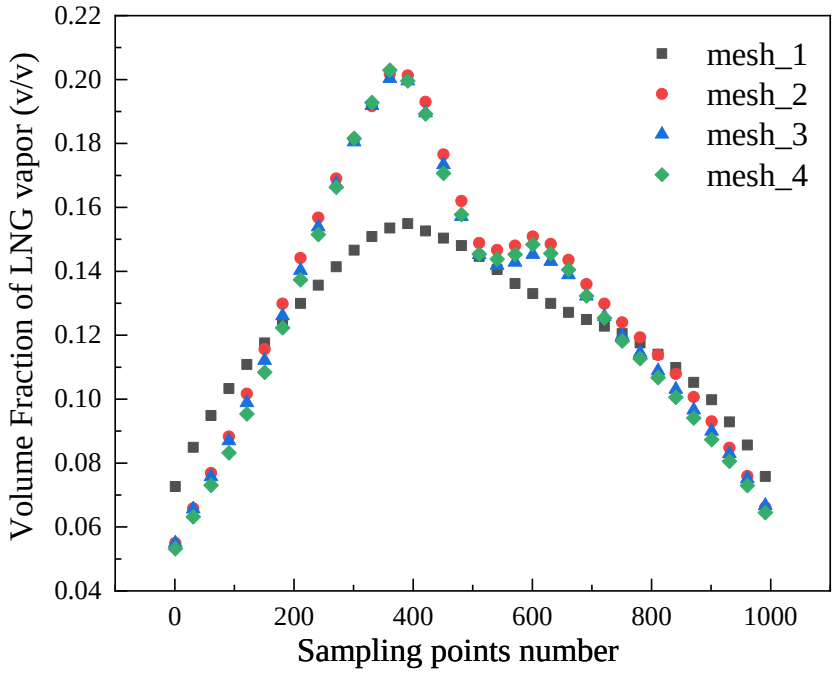

Fig.3 LNG vapor volume fraction at sampling line

Fig.4 presents the horizontal concentration distribution of the LNG vapor at the height of 1 m after LNG spilling. It shows the LNG vapor contours of 1%, 2%, 5%, 10%, 15%, 25%, and 35% volume fraction. The results show that a gravity-driven gas cloud moved downwind as time goes by under the stable atmosphere stability in the Burro 8 test. Furthermore, the shapes of the gas cloud obtained from the field test have less symmetry about the center-line of the computational domain compared with the simulation results. The reason for this may be that there was a non-uniform wind speed in different directions existing in the field test, which was ignored in the CFD simulations. However, the lateral and downwind range of the vapor dispersion of the OpenFOAM code results was in a good agreement with the field test and the ANSYS FLUENT simulation, which demonstrates that the OpenFOAM code well reproduced the distribution of the LNG vapor dispersion and can be used as an alternative tool for LNG vapor dispersion with good reliability.

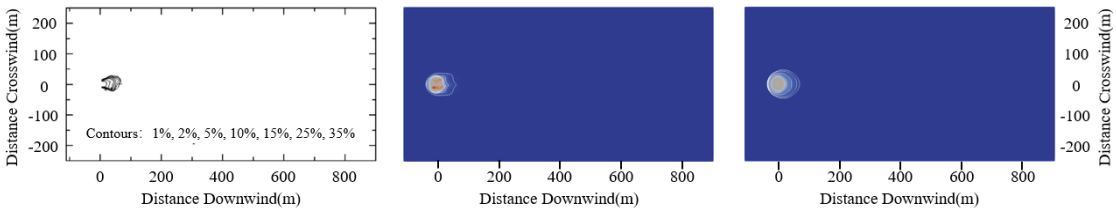

20 s field test 20 s OpenFOAM 20 s FLUENT

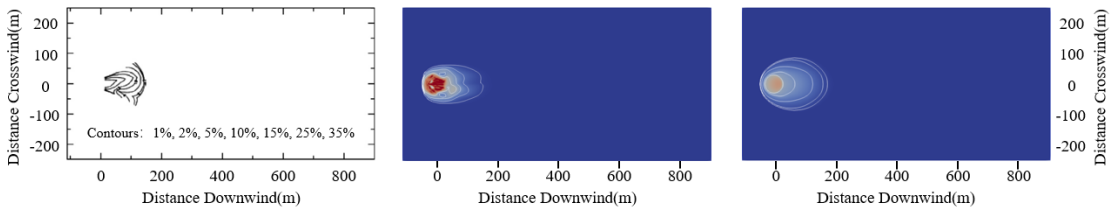

60 s field test 60 s OpenFOAM 60 s FLUENT

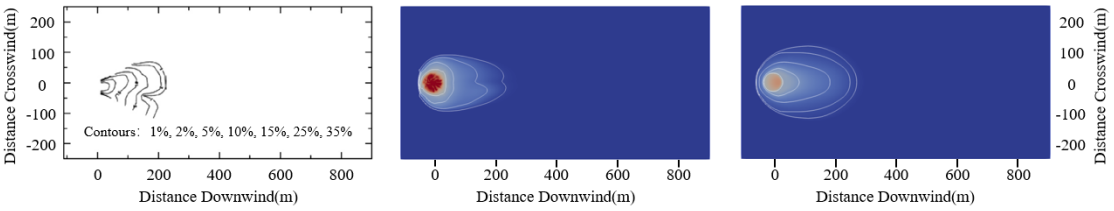

100 s field test 100 s OpenFOAM 100 s FLUENT

Fig.4 LNG vapor contours at olume fraction of 1%, 2%, 5%, 10%, 15%, 25%, and 35%

3.2 LNG vapor dispersion in receiving terminal

Different from the experimental data investigated above, the LNG vapor dispersion process in the LNG receiving terminal will be influenced by complex obstacle layouts, ambient ventilation conditions, buoyancy forces and so on. In order to investigate the LNG vapor cloud dispersion in receiving terminal at ports, a typical LNG receiving terminal located in the north of China was selected as simulation scenario in this section.

3.2.1 Numerical configurations of LNG port model

In this section, the computational domain has a dimension of 1120_m×880_m×100_m, and the leakage hole is placed at the center of the computational domain. The layout and the boundary conditions of the investigated

LNG receiving terminal model are shown in **Fig.5.** Meanwhile, the detailed parameters of the LNG receiving terminal model are presented in **Table.2**.

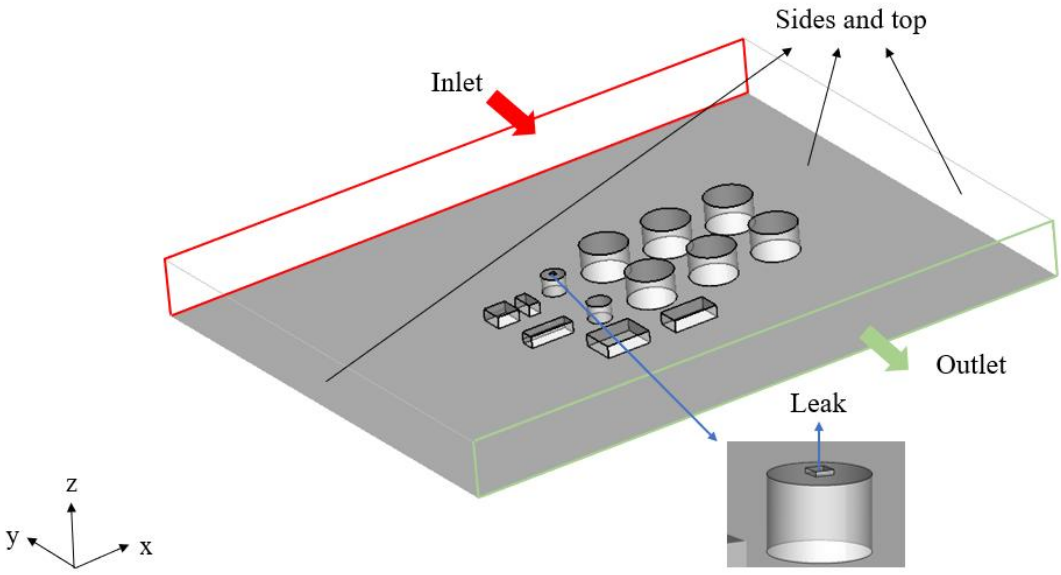

Fig.5 The layout and boundary conditions of the investigated LNG receiving terminal at ports

Table 2 Configurations of the investigated LNG receiving terminal model

Parameter	value
Width (m)	220
Height (m)	50
Length (m)	280
Average flow speed in inlet (m/s)	8
Leakage area (m^2)	64
Leakage velocity of LNG (m/s)	15
Location of leakage source (m)	(500 m, 20 m, 32 m)
Environment temperature (K)	298
Density of LNG at the leak hole (kg/m3)	1.76

Temperature of LNG at the leak hole (K)	111.

The computational domain above was created and discretized by using ANSYS ICEM. Three meshes with different grids (20 thousand, 40 thousand, and 60 thousand) were used for primary simulations and comparisons. It showed that there was a small average relative error that was 0.048 between the results of mesh_2 with 40 thousand grids and mesh_3 with 60 thousand grids. However, the errors between the results of mesh_2 and mesh_1 with 20 thousand grids can not be ignored, being 0.20. Therefore, mesh_2 was selected for the following simulations with better accuracy and computing speed. Moreover, a wind field under steady-state was calculated and initialed in the simulation of LNG vapor leakage and dispersion in the LNG receiving terminal in order to ensure a more realistic leakage scenario.

The boundary conditions applied in the simulation are shown as follows:

(ⅰ) Inlet: A power law correlation velocity was utilized in the air inlet boundary, which was calculated by formula (21). And the z_0 and u_0 were set as 3 m/s and 2 m respectively according to the meteorological records of northern China. Additionally, the λ was set as 0.4 with consideration of the layout of the complex buildings.

(ⅱ) Leak: The leakage velocity of the LNG vapor was set as 15 m/s under the assumption that the LNG was easy to evaporate and accumulate in the higher part of the storage tank. The temperature of the leaked LNG vapor at the leak hole was set as 111 K.

(iii) Outlets: The fully developed condition was employed in the outlets as outflow conditions.

(iv) Sides and top: Two sides and the top of the computational domain were defined as symmetry conditions.

(v) Walls: All the walls and blocks in the investigated model were set as no-slip wall conditions.

3.2.2 LNG vapor dispersion analysis

The simulation of LNG vapor leakage and dispersion in the LNG receiving terminal at ports was presented to investigate the characteristics of the LNG cloud dispersion. Due to the high molecular weight, the low temperature, and the presence of the aerosols, some released materials usually have the density that is heavier than the ambient gas and will be driven by the gravity (Pontiggia et al., 2009). The LNG vapor usually leaked and dispersed as dense gas at the initial stage before the temperature rose because of the cryogenic storage condition. However, with the exchange of heat between leaked LNG vapor and the surrounding atmospheric environment, the leaked LNG vapor will be heated and behave like light gas gradually. Therefore, the leakage and dispersion process of the LNG vapor is complex, especially in the environment with some obstacles, which increases the complexity of the airflow. In this section, the horizontal and vertical distributions of the LNG vapor are presented in **Fig.6** and **Fig.7**.

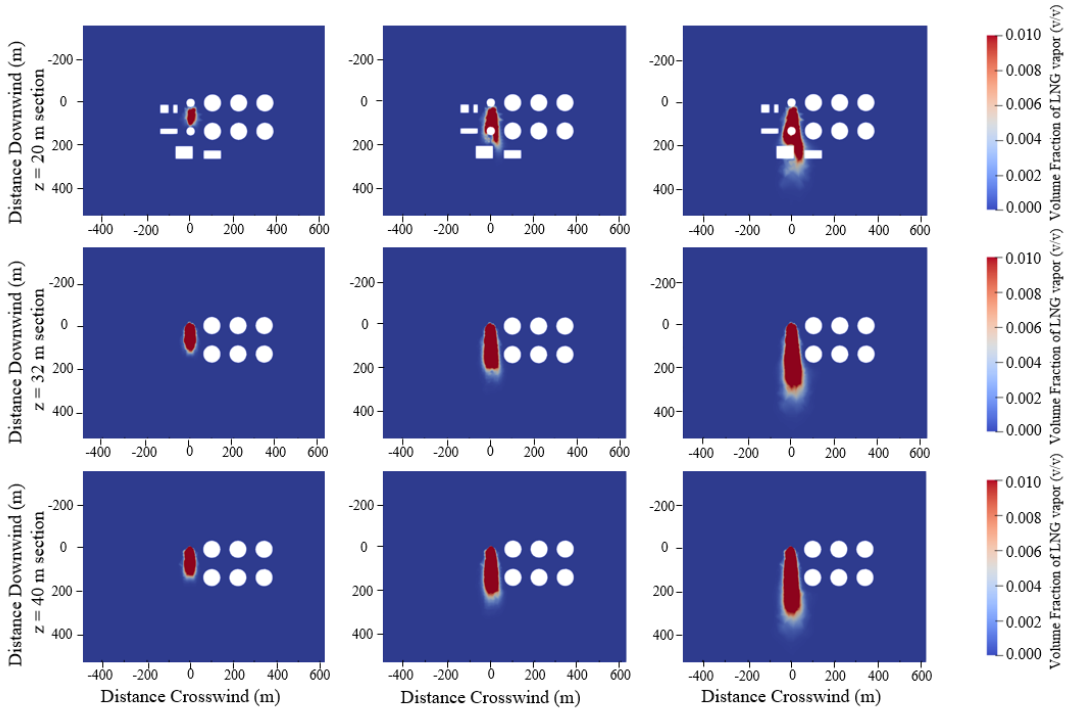

Fig.6 Horizontal concentration distribution of LNG vapor at Z=20 m, Z=32 m and Z=40 m sections

Fig.6 compares the horizontal concentration distributions of the LNG vapor at different horizontal section heights (Z=20 m, Z=32 m and Z=40 m) at 10 s, 20 s and 30s. The range of the leaked LNG vapor in the Z=20 m section was smaller than the Z=32 m and Z=40 m sections due to the delay of the LNG vapor dispersion, lower ambient wind speed and the complex obstacles. Since the effects of the obstacles could lead to a low wind velocity at the leeward side of the storage tank, there was an obvious low concentration region at 150 m downwind in the Z=20 m section at 20 s and 30 s. Whereas, the LNG vapor cloud in the Z=32 m and Z=40 m sections had similar range areas because the there was no obstacle that could influence the process of vapor cloud dispersion in the direction of wind flow. Moreover, the vapor cloud range of the z=40

m section was slightly greater than z=32 m section, and it was probably because the applied pow law correlation inlet made a relatively higher wind velocity in the z = 40 m section.

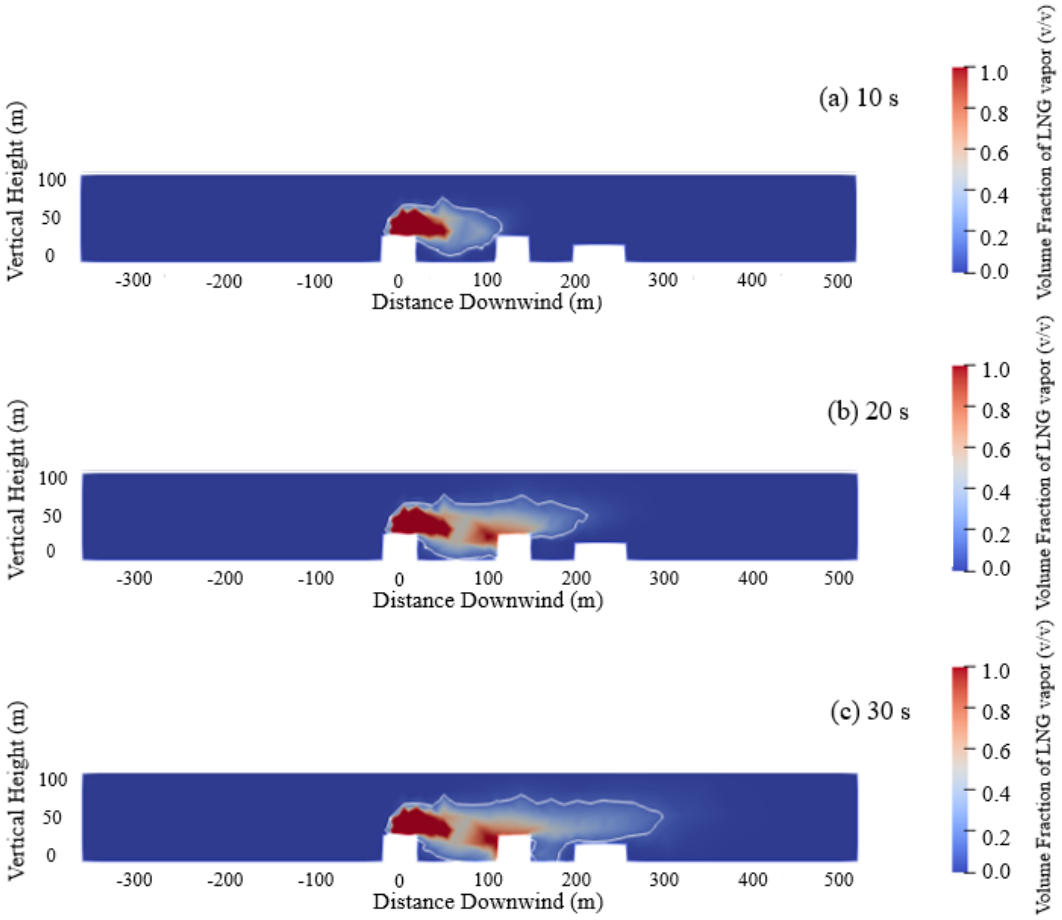

Fig.7 Vertical concentration distribution of LNG vapor at X=500 m section

The concentration distributions of the LNG vapor in vertical section were presented in the **Fig.7**. At the initial stage of LNG vapor leakage, the vapor cloud dispersion was mainly dominated by the leakage velocity and the wind speed near the leakage source, and then the cryogenic dense vapor cloud affected by the gravity had the tendency to sink as shown in panel (a). After spreading out of leakage source area,

369 the buoyant force and the obstacles would have more influence on the vapor cloud
370 dispersion gradually. A conspicuous dipped trajectory of vapor cloud could be seen
371 between the first two tanks and a certain amount of LNG vapor sank into the cavity area
372 in panel (b) and panel (c). A relatively high concentration of LNG vapor could be seen
373 near the top of the second tank at 100 m downwind in panel (b) and panel (c). That was
374 because there were vortexes in the cavity area between the two tanks caused by the
375 LNG receiving terminal layout, and the similar phenomenon of vapor cloud dispersion
376 could be seen in the street canyons (Liu et al., 2018). The LNG vapor cloud continued
377 to spread to around 300 m downwind without obvious sinking trend, it was probably
378 because the density of the LNG vapor decreased gradually with the heat transfer
379 between LNG vapor cloud and the atmospheric environment. Therefore, the vapor
380 cloud dispersion process became momentum-dominated after 300 m downwind in
381 panel (c).

382 **3.3 CFD and EnKF coupling estimation of LNG leakage and dispersion**

383 In this paper, the twin experiment was used to validate the proposed CFD and
384 EnKF coupling prediction model for LNG vapor leakage and dispersion. Twin
385 experiment was widely used in the evaluation of data assimilation models (Bengtsson
386 et al., 1981, Ngodock and Carrier, 2013). There is always a control group in the twin
387 experiment, in which the numerical simulations with controlled initial parameters can
388 be used and the simulation of section 3.2 was employed as the control group in this
389 paper.

3.3.1 Configurations of the CFD and EnKF coupling model

In the CFD and EnKF coupling model, the observation sampling time step was set as 0.5 s, which means the observation data from the control group will be utilized for data assimilation every 0.5 s. We set up 100 observation sites in the control group simulation to obtain observation data of the LNG vapor concentration. The ensemble size in the CFD and EnKF coupling model was set as 120 and the inflation factor (Anderson, 2007) was set as 1.0 in this paper. Additionally, two parameters with uncertainties were taken into account in the proposed model: the initial-guess leakage velocity and the airflow velocity in the computational domain. We set the initial-guess leakage velocity as an ensemble following uniform distribution from 0 m/s to 10 m/s, whereas the actual leakage velocity was 15 m/s, which is shown in **Fig. 8.** The u ensemble calculated in the CFD and EnKF coupling model was presumed to follow a normal distribution of $N(1, 0.1)$. We selected 100 observation sites in three sections of the computational domain, 9 observation sites in the Z=20 m section, 70 observation sites in the Z=32 m section and 21 observation sites in the X=500 m section respectively. The layouts of the observation sites are shown in **Fig. 9.** The detailed configurations of the CFD and EnKF coupling model are shown in **Table 3**.

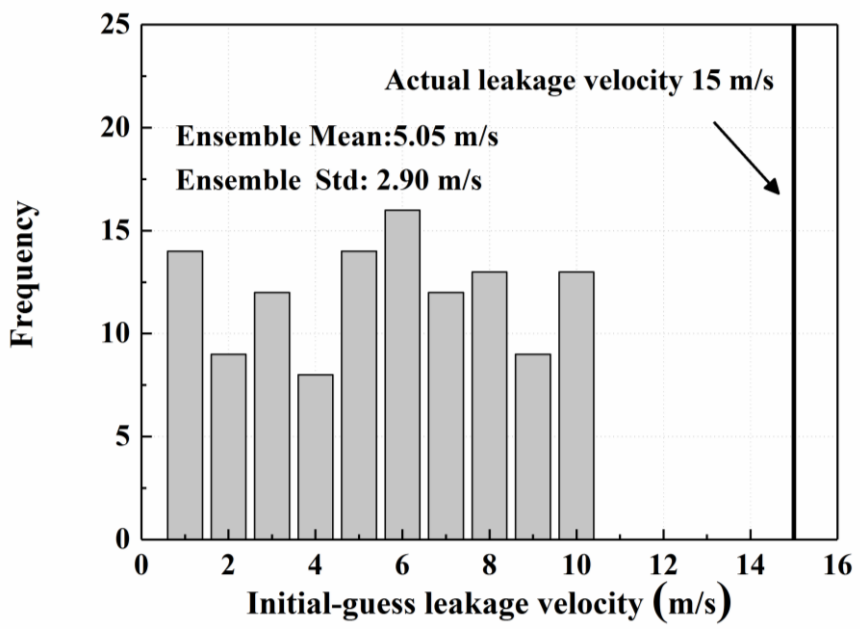

407

408 **Fig. 8.** The initial-guess leakage velocity ensemble used in the CFD and EnKF coupling
409 model

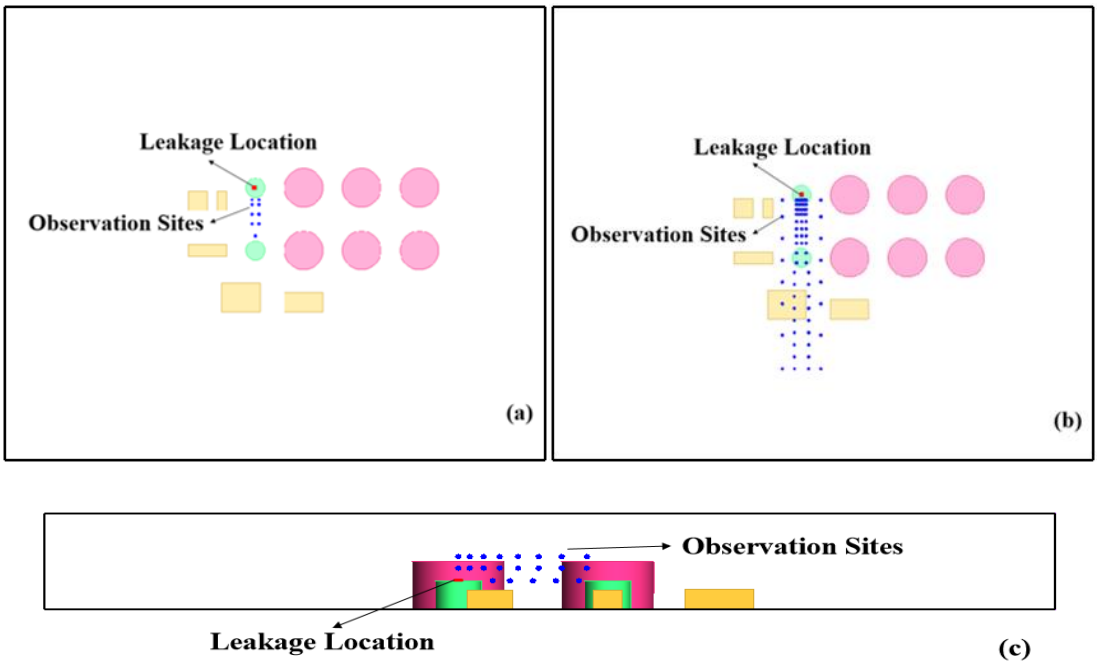

410

411

412 **Fig. 9.** The layouts of the observation sites in three sections of the computational domain: (a)
413 Z=20 m section, (b) Z=32 m section and (c) X=500 section

414 **Table 3** Configurations of the CFD and EnKF coupling model

Parameter	Setup value

Ensemble number	120
Ensemble inflation	1.0
Number of measurement sites	100
Observation time interval (s)	0.5
Perturbation of velocity ensemble	N (1, 0.1)
Number of observation time steps	100

3.3.2 Predictions of the CFD and EnKF coupling model

Fig.10 to **Fig.12** illustrate the comparisons between the horizontal concentration distributions of the LNG vapor cloud at three different sections calculated by the control group, data assimilation group and a reference group without data assimilation (the leakage velocity in the this group was set as 5 m/s for reference). Moreover, we investigated the effectiveness of the proposed model by using three horizontal sections with different numbers of observation sites, 9 observation sites in the Z=20 m section, 30 observation sites in the Z=32 m section and 0 observation sites in the Z=40 m section.

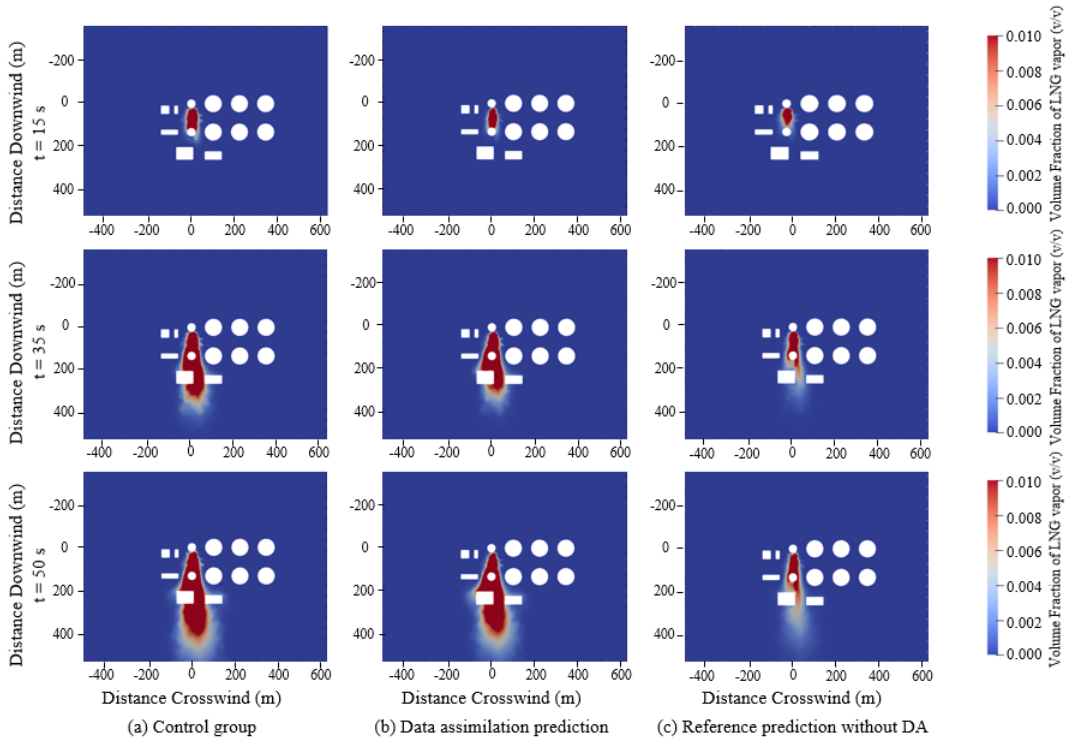

Fig.10 Horizontal concentration distribution of LNG vapor at Z=20 m section

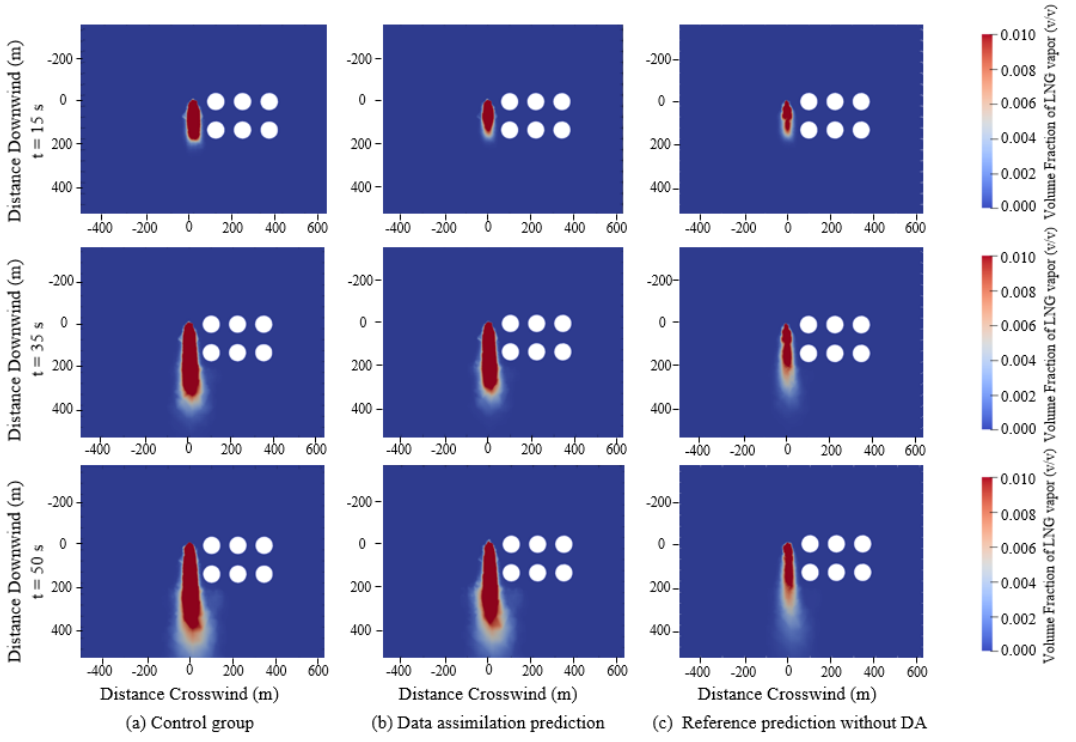

Fig.11 Horizontal concentration distribution of LNG vapor at Z=32 m section

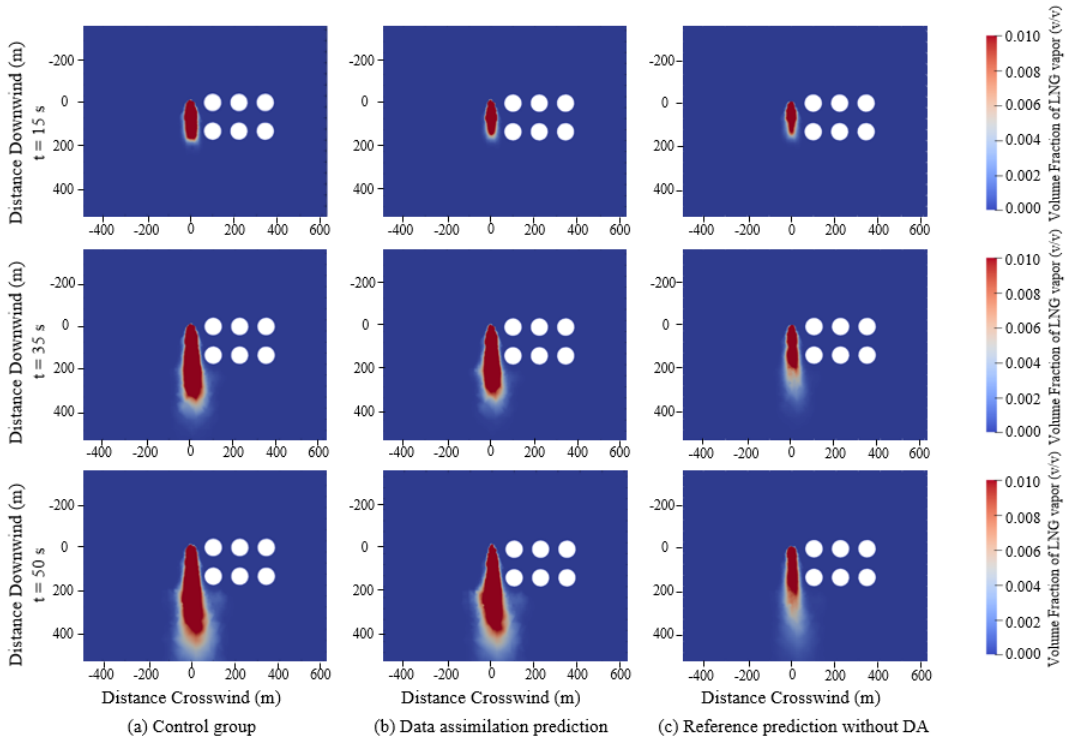

Fig.12 Horizontal concentration distribution of LNG vapor at Z=40 m section

The concentration distributions of LNG vapor at three different horizontal sections calculated by three different simulation groups can be seen in **Fig.10** to **Fig.12.** At the initial stage of vapor leakage and dispersion, there was no obvious difference of LNG vapor distribution range area between the data assimilation prediction and the reference prediction without DA due to the fact that the leakage velocity used in the two groups was similar. The LNG vapor distributions in three sections of the control group were slightly larger than the two predictions at 15 s because the underestimation of the leakage velocity in two prediction groups led to the underestimation of the LNG vapor distribution area. The correlation coefficients between the data assimilation prediction and the reference prediction without DA and the control group distribution at the observation sites are respectively 0.93 and 0.75 at 15 s. As time goes on, the difference

of LNG vapor distribution between the control group and the reference prediction without DA increased gradually because of the difference existing in the vapor leakage velocity. However, the data assimilation group obtained the LNG vapor distribution predictions with good similarities compared with the actual LNG vapor distribution in the control group at 35 s and 50 s, in which the correlation coefficients between the data assimilation prediction and the control group at the observation sites are 0.98 and 0.96 respectively. Meanwhile, the correlation coefficient between the reference prediction without DA and the control group at the observation sites is only 0.48 in the end. That was because the observation data were used to correct the errors in the data assimilation prediction gradually and finally achieve the prediction of LNG vapor distribution with relatively high accuracy by the CFD and EnKF coupling model. Additionally, the LNG vapor distribution predictions in the three sections calculated by the CFD and EnKF coupling model were all comparable to the actual distributions in the control group, which means that the CFD and EnKF coupling model could realize the correction of the LNG vapor distribution in the whole computational domain even in the section without observation site.

Fig.13 presents the vertical concentration distribution of the LNG vapor cloud at X=500 m section calculated by the control group, the data assimilation group and the reference prediction group. The effectiveness of the proposed CFD and EnKF coupling model in the prediction of the LNG vapor vertical distribution could also be witnessed in **Fig.13**. After several data assimilation periods, the prediction of the LNG vapor

vertical distribution became more comparable to the actual distribution in the control group by using the CFD and EnKF coupling model. The correlation coefficients between the data assimilation prediction and the control group at the observation sites in the X=500 m section are 0.99 at 35 s and 0.98 at 50 s, which means the observation data in the X=500 m section was utilized by the CFD and EnKF coupling model effectively. Whereas, the reference prediction without data assimilation was quite different from the actual distribution during the whole calculation period and with the correlation coefficient of -0.06 in the end.

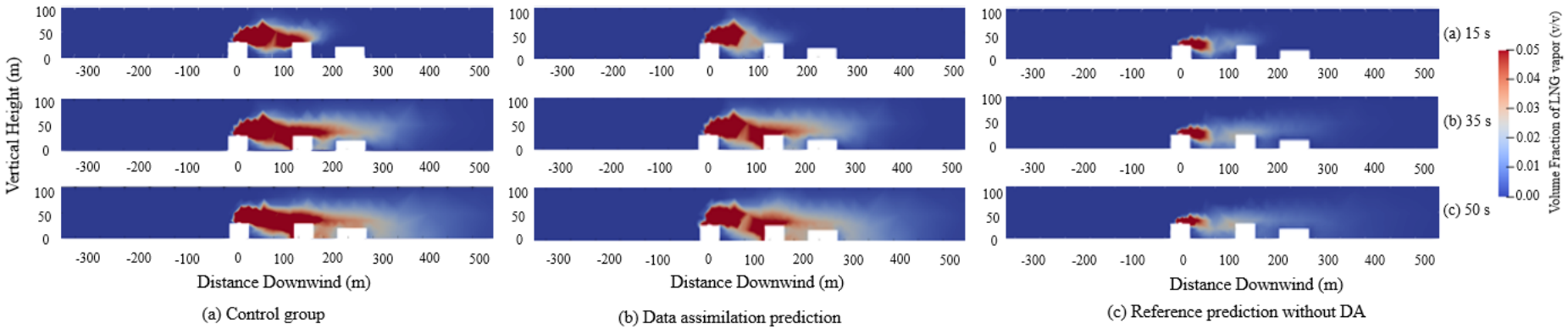

Fig.13 Vertical concentration distribution of LNG vapor at X=500 m section

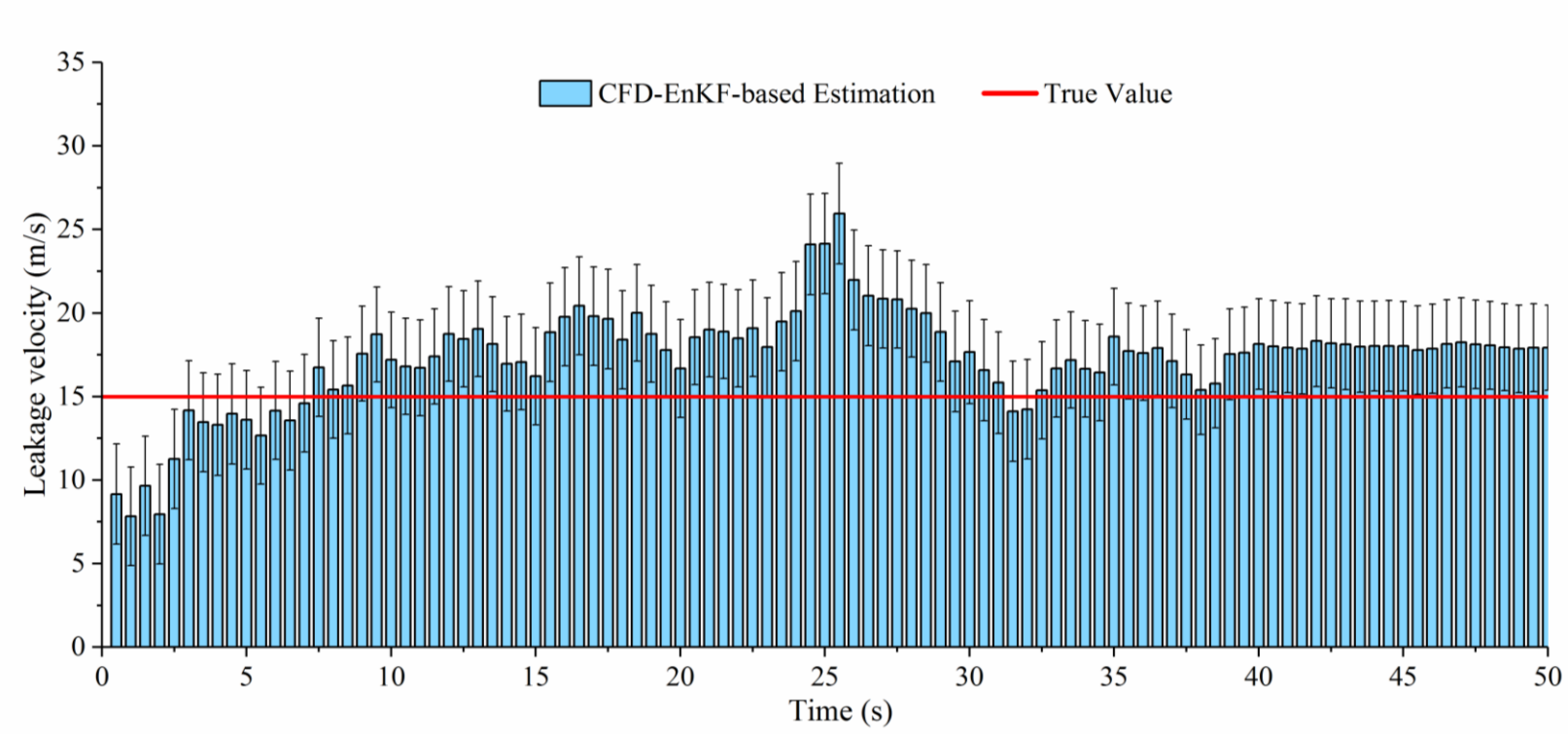

Fig.14 Leakage velocity estimation of the CFD and EnKF coupling model

Fig.14 presents the leakage velocity estimation process of the LNG vapor at the leak hole by the proposed CFD and EnKF coupling model. The underestimation of leakage velocity can be seen at the initial period of time in **Fig.14.** That was because the underestimation existing in the initial-guess leakage velocity had some influence on the leakage velocity estimation and led to the errors of leakage velocity estimation at the initial several data assimilation periods. However, the overestimation of leakage velocity happened until around 30 s due to the overcorrection of the initial-guess leakage velocity caused by the data assimilation process. Finally, the estimation of leakage velocity became stable at around 18 m/s despite some fluctuations. The mean relative error between the leakage velocity estimation and the true value was 24.6 % from start to 30 s and the mean relative error of the leakage velocity estimation became 16.1 % from 30 s to the end due to the estimation of leakage velocity became stable gradually after 30 s. Therefore, we come to a conclusion that the proposed CFD and EnKF coupling model could be used to provide a reasonable estimation of LNG vapor leakage velocity with a high similarity to the actual leakage velocity despite there are huge errors existing in the initial-guess leakage velocity.

4. Conclusion

In this paper, a three-dimensional CFD and EnKF coupling model was proposed with the combination of CFD simulation and data assimilation technique, which is of potentials to provide more accurate LNG vapor distributions and source term estimations for emergency response and safety control of LNG vapor leakage accidents.

The main conclusions of this paper are presented below:

a) An OpenFOAM-based model was evaluated and validated in the simulation of LNG vapor leakage and dispersion by the Burro 8 spill test. The results show that the rhoReactingBuoyantFoam solver is effective in the simulation of LNG vapor dispersion compared with the experimental data and the ANSYS FLUENT results, which can be used as an alternative tool for simulating LNG vapor dispersion.

b) At the initial stage of LNG leakage, the process of LNG vapor dispersion in the LNG receiving terminal is dominated by the leakage velocity and the wind speed. Later, the natural wind velocity, buoyancy forces and the complex obstacle layouts will have a significant influence on the characteristics of the LNG vapor dispersion. The spreading features of the dense vapor driven by the wind field and the gravity can be well captured by the proposed CFD solver.

c) The proposed three-dimensional CFD and EnKF coupling model can obtain high-confidence prediction of spatiotemporal distribution of leaked LNG vapor and realize the reasonable estimation of LNG vapor leakage velocity. The effectiveness of the LNG vapor distribution predictions in the horizontal and vertical sections with different number of observation sites was evaluated with good reliability. Moreover, the estimation of leakage velocity can be obtained with acceptable errors after a period of data assimilation by the proposed model, which could be useful to provide leakage source information for decision-makers.

With the development and popularity of the supercomputer and the high-performance computing (HPC) technique, the computational efficiency of the proposed CFD and EnKF coupling model would be significantly improved, which helps to achieve a more timely source term estimation and LNG vapor distribution prediction. Additionally, machine learning is also a promising technique that can realize timely prediction of LNG vapor leakage and estimation of the leakage source by combining with the proposed model, which can be employed to generate huge data with high-confidence for model learning.

Acknowledgements

This work was supported by the National Key Research and Development Program of China (Grant No. 2017YFC0805001), the Beijing Nova Program (Grant No. 471 Z201100006820072), the Yue Qi Young Scholar Program of China University of Mining & Technology, Beijing, and the Chinese Scholarship Council (Grant No: 202006430007).

References

Baalisampanga, T., Abbassi, R., Garaniya, V., et al., 2019. Modelling an integrated impact of fire, explosion and combustion products during transitional events caused by an accidental release of LNG. Process Safety and Environmental Protection. 128,259-272.

Bengtsson L, Ghil M, Källén E. Dynamic Meteorology: Data Assimilation Methods. Springer New York 1981.

Burro Series Data Report, 1982. LLNL/NWC Report No.UCID-19075, v.1 2. Berkeley. CA: Lawrence Livermore National Laboratory.

Cormier, B.R., Qi, R., Yun, G., et al, 2009. Application of computational fluid dynamics for LNG vapor dispersion modeling: A study of key parameters. Journal of Loss Prevention in the Process Industries. 22, 332-352.

Coyote Series Data Report, 1983. LLNL/NWC, UCID-19953. 1 2.

Dasgotra, A., Teja, G., Sharma, A., et al., 2018. CFD modeling of large-scale flammable cloud dispersion using FLACS. Journal of Loss Prevention in the Process Industries. 56,531-536.

Falcon Series Data Report, 1990. Gas Research Institute, 1987 LNG Barrier Verification Field Trials, GRIReport No.89/0138, Chicago, IL.

Fiates, J., Vianna, S., 2016. Numerical modelling of gas dispersion using Open FOAM. Process Safety and Environmental Protection. 104,277-293.

Giannissi, S.G., Venetsanos, A.G., Markatos, N., et al., 2013. Numerical simulation of LNG dispersion under two-phase release conditions. Journal of Loss Prevention in the Process Industries. 26, 245-254.

Guo, D., Zhao, P., Wang, R., et al., 2019. Numerical simulation studies of the effect of atmospheric stratification on the dispersion of LNG vapor released from the top of a storage tank. Journal of Loss Prevention in the Process Industries. 61,275-286.

Ji, J., Tong, Q., Wang, L., et al., 2018. Application of the EnKF method for real-time forecasting of smoke movement during tunnel fires. Advances in Engineering Software. 115,398-412.

Lee, C., Lim, Y., Han, C., 2012. Operational strategy to minimize operating costs in liquefied natural gas receiving terminals using dynamic simulation. K

546 orean J. Chem. Eng. 29(4), 444-451.

547 Li, X.J., Zhou, R.P., Konovessis, D., 2016. CFD analysis of natural gas dispers
548 ion in engine room space based on multi-factor coupling. Ocean Engineerin
549 g. 111, 524-532.

550 Li, Y., Chen, X., Chein, M.H., 2012. Flexible and cost-effective optimization of
551 BOG (boil-off gas) recondensation process at LNG receiving terminals. Ch
552 emical Engineering Research and Design. 90, 1500-1505.

553 Lin, C.C., Wang, L., 2013. Forecasting simulations of indoor environment using
554 data assimilation via an Ensemble Kalman Filter. Building and Environmen
555 t. 64,169-176.

556 Liu, A.H., Huang, J., Li, Z.W., et al., 2018. Numerical simulation and experim
557 ent on the law of urban natural gas leakage and diffusion for different buil
558 ding layouts. Journal of Natural Gas Science and Engineering. 54, 1-10.

559 Luo, T., Yu, C., Liu, R., et al, 2018. Numerical simulation of LNG release an
560 d dispersion using a multiphase CFD model. Journal of Loss Prevention in
561 the Process Industries. 56,316-327.

562 Mack, A., Spruijt, M., 2013. Validation of OpenFoam for heavy gas dispersion
563 applications. Journal of Hazardous Materials. 262, 504-516.

564 Ngodock H, Carrier M. A weak constraint 4D-var assimilation system for the
565 navy coastal ocean model using the representer method// data assimilation f
566 or atmospheric, oceanic and hydrologic applications (Vol. II). Springer Berli
567 n Heidelberg 2013: 367-390.

568 Pontiggia, M., Derudi, M., Busini, V., et al., 2009. Hazardous gas dispersion: a
569 CFD model accounting for atmospheric stability classes. J. Hazard. Mater.
570 171, 739-747.

571 Pu, Z., Hacker, J., 2009. Ensemble-based Kalman filters in strongly nonlinear d
572 ynamics. Progress in Atmospheric Science. 26(3), 373-380.

573 Qi, R., Ng, D., Cormier, B.R., et al, 2010. Numerical simulations of LNG vap
574 or dispersion in Brayton Fire Training Field tests with ANSYS CFX. J. Ha
575 zard. Mater. 183, 51-61.

576 Sklavounos, S., Rigas, F., 2006. Simulation of Coyote series trials—Part I: CF
577 D estimation of non-isothermal LNG releases and comparison with box-mod
578 el predictions. Chemical Engineering Science. 61, 1434-1443.

579 Siddiqui, M., Jayanti, S., Swaminathan, T., 2012. CFD analysis of dense gas di
580 spersion in indoor environment for risk assessment and risk mitigation. Jour
581 nal of Hazardous Materials. 209-210, 177-185.

582 Sun, B., Utikar, B.P., Pareek, V.K., et al, 2013. Computational fluid dynamics
583 analysis of liquefied natural gas dispersion for risk assessment strategies. Jo
584 urnal of Loss Prevention in the Process Industries. 26,117-128.

585 Valdes-Abellan, J., Pachepsky, Y., Martinez, G., 2018. MATLAB algorithm to i
586 mplement soil water data assimilation with the Ensemble Kalman Filter usin
587 g HYDRUS. MethodsX. 5,184-203.

588 Wu, J.S., Yuan, S.Q., Zhang, C., et al., 2018. Numerical estimation of gas rele
589 ase and dispersion in coal mine using Ensemble Kalman Filter. Journal of
590 Loss Prevention in the Process Industries. 56, 57-67.

591 Xing, J., Liu, Z.Y., Huang, P., et al., 2013. Experimental and numerical study
592 of the dispersion of carbon dioxide plume. Journal of Hazardous Materials.
593 256-257, 40-48.

594 Xue F., Kikumoto H., Li X., et al., 2018. Bayesian source term estimation of
595 atmospheric releases in urban areas using LES approach. Journal of Hazard

ous Materials. 349,68-78.

Yuan, S.Q., Wu, J.S., Zhang, X.L., et al., 2019. EnKF-based estimation of natural gas release and dispersion in an underground tunnel. Journal of Loss Prevention in the Process Industries. 62,103931.

Zhang, X., Huang M., 2017. Ensemble-based release estimation for accidental river pollution with known source position. Journal of Hazardous Materials. 333,99-108.

Zhang, X., Li, J., Zhu, J., et al., 2015. Computational fluid dynamics study on liquefied natural gas dispersion with phase change of water. International Journal of Heat and Mass Transfer. 91,347-354.

Zhang, X.B., Li, J.F., Zhu, J.K., et al., 2015. Computational fluid dynamics study on liquefied natural gas dispersion with phase change of water. International Journal of Heat and Mass Transfer. 91, 347-354.

Zhang, X.L., Su, G.F., Yuan, H.Y., et al., 2014. Modified ensemble Kalman filter for nuclear accident atmospheric dispersion: Prediction improved and source estimated. J. Hazard. Mater. 280, 143-155.

Zhang, X.L., Li, Q.B., Su, G.F., et al., 2015a. Ensemble-based simultaneous emission estimates and improved forecast of radioactive pollution from nuclear power plant accidents: application to ETEX tracer experiment. Journal of Environmental Radioactivity. 142,78-86.

Zhang, X.L., Su, G.F., Chen, J.G., et al., 2015b. Iterative ensemble Kalman filter for atmospheric dispersion in nuclear accidents: An application to Kincaid tracer experiment. Journal of Hazardous Materials. 297,329-339.